NATIONAL UNIVERSITY OF SCIENCES AND TECHNOLOGIES POLITEHNICA BUCHAREST

Doctoral School of Electronics, Telecommunications and Information Technology

Decision No. 202 **from** 21-09-2024

Ph.D. THESIS SUMMARY

Mobina KEYMASI

METODE ADAPTIVE PENTRU RECUNOAȘTEREA ȘI CLASIFICAREA IMAGINILOR SAR

GOAL-DIRECTED COMPRESSIVE RADAR IMAGING

THESIS COMMITTEE

Prof. dr. ing. Gheorghe BREZEANU National University of Sciences and Technologies POLITEHNICA Bucharest	President
Prof. Dr. Ing. Mihai DATCU National University of Sciences and Technologies POLITEHNICA Bucharest	PhD Supervisor
Prof. Univ. Dr. Habil. Ing. Cătălin Daniel CĂLEANU University Politehnica Timisoara	Referee
Conf. dr. ing. Ștefan-Adrian TOMA Military Technical Academy "Ferdinand I"	Referee
Prof. Dr. Ing. Habil. Andrei ANGHEL National University of Sciences and Technologies POLITEHNICA Bucharest	Referee

BUCHAREST 2024

Table of contents

Chapter 1

Introduction

Remote Sensing (RS) enables non-invasive monitoring of Earth's surface, atmosphere, and oceans through electromagnetic radiation (EMR) analysis [5, 29]. It supports environmental monitoring, urban planning, disaster response, and resource management, especially via Synthetic Aperture Radar (SAR) for high-resolution imagery regardless of weather [31]. To address RS data challenges, Compressive Sensing (CS) reduces data acquisition needs, enhancing real-time applications [1, 7]. Integrating AI, particularly Machine Learning (ML) and Deep Learning (DL), further automates RS data processing, boosting efficiency for Earth observation [7].

1.1 Fundamentals of RS

RS captures data by analyzing EMR interactions with Earth's surface. Modern RS spans multiple spectral bands, detecting phenomena beyond visual perception. Key components include platforms, sensors, and data processing systems, advancing weather forecasting and emergency response [5].

1.1.1 Types of RS

- **Passive RS**: Captures natural radiation, used for vegetation and land cover studies [29].
- **Active RS**: Emits energy to measure reflections; SAR provides topographic details useful in mapping and monitoring [31].

1.2 RS Platforms

RS data collection platforms include:

- **Satellites**: Provide global monitoring, essential for environmental studies [17].

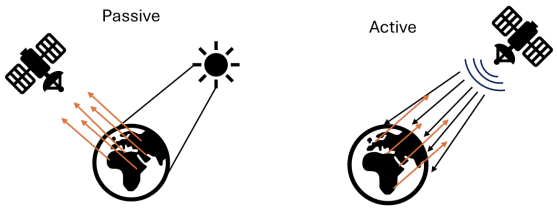

Fig. 1.1 Comparison of Active vs. Passive RS systems.

- **Aircraft and Drones**: Allow localized, high-resolution applications, e.g., precision agriculture [29].

1.3 Applications of RS

Key RS applications:

- **Environmental Monitoring**: Observes deforestation and pollution [5].
- **Urban Development**: Assesses land use and post-disaster infrastructure [31].
- **Agriculture**: Monitors crop health, optimizing resource use [29].

1.4 Electromagnetic Spectrum

RS uses various wavelengths, each providing insights into Earth's features for detailed analysis [5, 29].

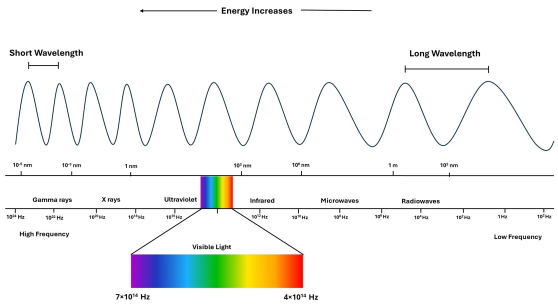

Fig. 1.2 The electromagnetic spectrum, showing wavelengths from gamma rays to radio waves. Multispectral RS typically utilizes visible and infrared portions, while SAR operates within longer microwave wavelengths.

1.5 Motivation and Importance

This research is motivated by the need to manage massive RS datasets, particularly from SAR, which require efficient storage and processing [1]. SAR's ability to capture detailed

Earth observation data generates large volumes that challenge traditional processing methods. This study explores Compressive Sensing (CS) to reduce data acquisition while preserving quality, enabling faster processing and reduced storage [7]. Integrating AI and ML further automates and enhances SAR data analysis, supporting global applications in climate change, resource management, and urban planning [31].

1.6 Scope of the Thesis

The thesis focuses on developing CS techniques for SAR imaging to minimize data requirements while maintaining resolution [7]. It also investigates ML and DL methods for advanced SAR data analysis.

Key areas include:

- Theoretical CS foundations and SAR applications [1].
- Techniques for reducing data redundancy in radar imaging [31].
- AI-based SAR data processing for feature extraction and detection [7].
- Applications in environmental and urban monitoring [5].
- Challenges of using CS in radar imaging [1].

1.7 Structure of the Thesis

The thesis is structured as follows:

- **Chapter 1: Introduction** - Overview of RS, CS, AI, and thesis structure.
- **Chapter 2: Earth Observation Data** - Types and applications of SAR and multispectral data.
- **Chapter 3: Data Processing** - CS and ML methods for feature extraction.
- **Chapter 4: CS in RS** - CS applications for SAR data.
- **Chapter 5: AI for SAR Analysis** - AI/ML techniques in SAR data processing.
- **Chapter 6: Experiments and Results** - Experimental setup and SAR data analysis results.
- **Chapter 7: Conclusion** - Summary and future research directions.

This structure provides a detailed exploration of how CS and AI can enhance radar-based RS for efficient Earth observation [5, 31].

Chapter 2

Information Content of Earth Observation

2.1 Introduction

This chapter explores the information content in Earth Observation (EO) systems, focusing on SAR and multispectral data. With advancements in Remote Sensing (RS), data volumes increase, requiring insights for decision-making. Key factors—**spatial**, **spectral**, **temporal**, and **radiometric resolutions**—determine data quality and applicability [29]. Case studies, such as tracking **lava flows** and monitoring **environmental changes** in the Danube Delta, demonstrate EO's adaptability [39, 25].

2.2 Importance of Information Content

EO data's value is enhanced by its **spatial**, **spectral**, **temporal**, and **radiometric resolutions,** improving analysis across applications.

2.2.1 Spatial Resolution

Spatial resolution is crucial for detecting small objects in urban and environmental contexts [5].

2.2.2 Spectral Resolution

Spectral resolution enables material differentiation; multispectral data supports agricultural monitoring with NDVI [33].

2.2.3 Temporal Resolution

Temporal resolution shows revisit frequency, important for monitoring dynamic environments [17].

2.2.4 Radiometric Resolution

Radiometric resolution captures intensity changes, aiding applications like soil moisture monitoring [5].

2.3 Overview of SAR and Multispectral Data

This section compares **SAR** and **multispectral** data for environmental monitoring, agriculture, and disaster response.

2.3.1 SAR Data

SAR provides high-resolution imagery for **disaster response** and **environmental monitoring** [17].

2.3.2 Multispectral Data

Multispectral sensors capture multiple bands, useful in agriculture, forestry, and land classification [5].

2.3.3 Comparative Analysis

- **Resolution**: SAR offers spatial detail; multispectral provides spectral depth [17].
- **Coverage**: SAR operates in all weather; multispectral requires clear skies [35].
- **Applications**: SAR suits structural monitoring; multispectral excels in vegetation and land use [29].

2.4 Processing and Case Studies

Processing SAR and multispectral data yields actionable insights, with applications in **lava monitoring** and **environmental conservation** illustrating EO's value.

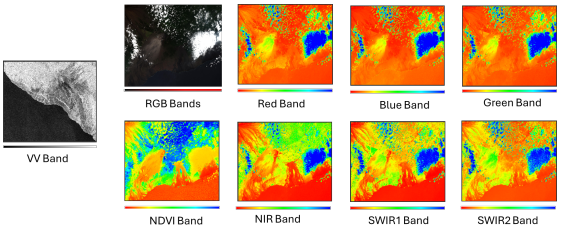

(a) Multispectral RGB composite image of the Kīlauea lava flow (July 22, 2018). The dark regions show the lava flow, vegetation is represented in green, and clouds are visible in white.

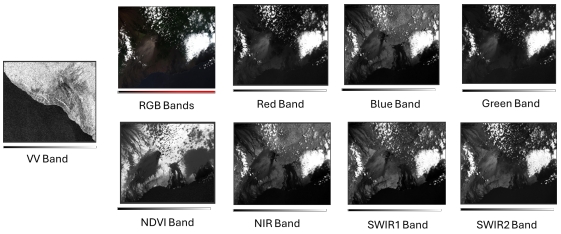

(b) SAR VV polarization image of the Kīlauea lava flow (July 31, 2018). Dark regions indicate fresh lava flows with smooth surfaces, while brighter areas correspond to rough volcanic terrain and vegetation.

Fig. 2.1 Combined analysis of the Kīlauea lava flow using SAR and multispectral data. The integration of these datasets highlights active lava areas and surface roughness.

2.4.1 Lava Monitoring: SAR and Multispectral Data

Lava monitoring aids in forecasting and safety, as shown in the 2018 Kīlauea eruption using SAR and multispectral data.

Multispectral sensors provide a broad range of wavelengths that are effective for detecting surface changes and thermal anomalies in volcanic regions. Figure 2.1 illustrates how SAR and multispectral data are used to track lava flows and analyze surface roughness during the Kīlauea eruption, providing valuable information for real-time hazard assessments.

2.4.2 Danube Delta Monitoring: SAR and Multispectral Data

The Danube Delta, a biodiversity hotspot, requires precise ecological monitoring, conservation, and management efforts. The combination of SAR and multispectral data provides detailed insights into land cover, vegetation, water quality, and ecological changes.

Figure 2.2 shows the integration of SAR and multispectral data to monitor vegetation health and water quality in the Danube Delta, supporting wetland conservation and restoration efforts.

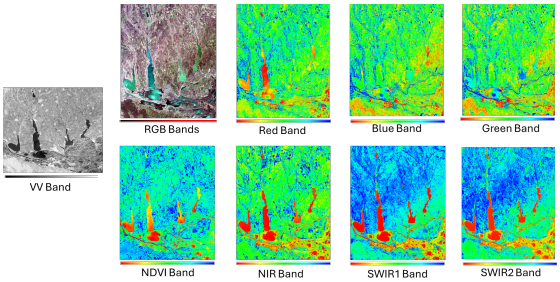

(a) Multispectral RGB composite of the Danube Delta using Sentinel-2 bands. Vegetation is shown in various shades of green, while water bodies appear in blue and turquoise.

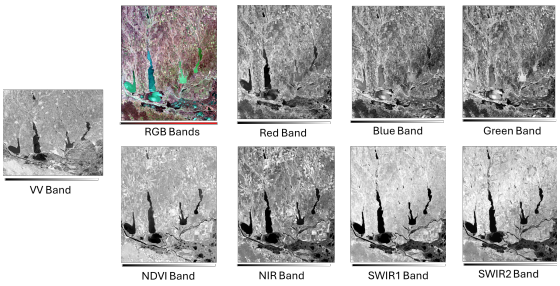

(b) SAR VV polarization image of the Danube Delta, providing a grayscale analysis of surface features. Brighter areas represent dense vegetation and rough surfaces, while darker regions indicate smooth water bodies.

Fig. 2.2 Combined analysis of the Danube Delta using Sentinel-2 multispectral bands and SAR data. The fusion of datasets reveals vegetation health and surface features.

2.4.3 Eyjafjallajökull Region Monitoring: SAR and Multispectral Data

The Eyjafjallajökull volcano in Iceland poses monitoring challenges due to its activity and complex terrain. Combining SAR and multispectral data offers insights into volcanic features, surface roughness, and thermal properties.

Figure 2.3 illustrates how the integration of SAR and multispectral data can be used to monitor volcanic activity and surface changes in the Eyjafjallajökull region, providing critical information for hazard assessment and mitigation.

2.4.4 Erbil Citadel Monitoring: SAR and Multispectral Data

The Erbil Citadel, an important archaeological site, benefits from non-invasive SAR and multispectral data, providing a comprehensive approach for detecting and analyzing buried structures.

Figure 2.4 shows how SAR and multispectral data can be used to uncover buried structures and analyze the surface of the Erbil Citadel, providing valuable insights for archaeological preservation.

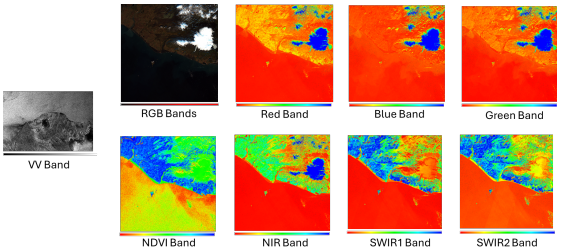

(a) Multispectral RGB composite of the Eyjafjallajökull region (October 2022). The volcanic terrain and surrounding vegetation are shown.

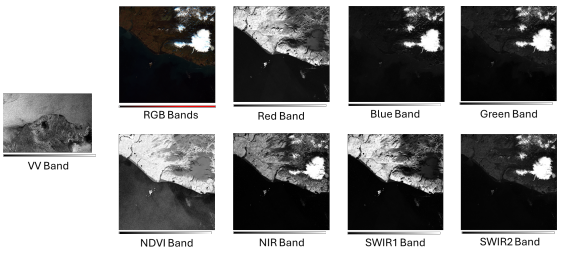

(b) SAR VV polarization image of Eyjafjallajökull (November 2022). Dark areas indicate recent lava flows with smooth surfaces, while brighter regions represent rough volcanic terrain.

Fig. 2.3 Combined analysis of the Eyjafjallajökull region using Sentinel-2 multispectral bands and SAR data. The fusion of datasets reveals volcanic activity and surface features.

(a) Multispectral RGB composite of the Erbil Citadel (December 2021). Vegetation and urban structures are shown in varying shades of green and brown.

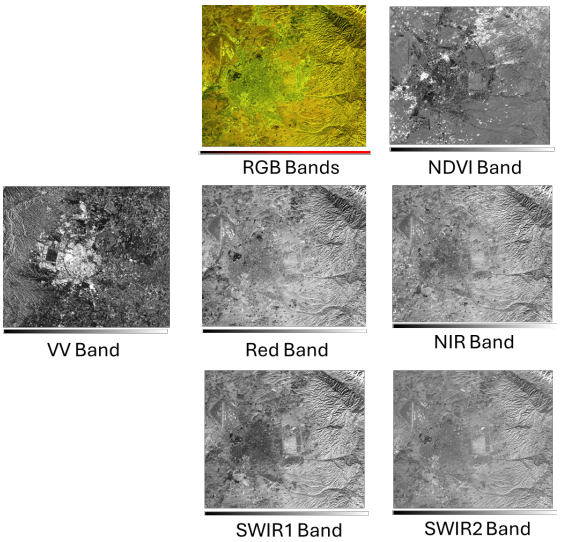

(b) SAR VV polarization image of the Erbil Citadel (December 2021). Brighter areas indicate rough terrain and subsurface structures, while smoother surfaces appear darker.

Fig. 2.4 Combined multispectral and SAR analysis of the Erbil Citadel using Sentinel-2 data. The fusion of datasets reveals subsurface structures and surface features.

2.4.5 Arctic Region Monitoring: SAR and Multispectral Data

The Arctic region, undergoing rapid environmental changes due to climate change, requires continuous monitoring. The combination of SAR and multispectral data is critical for tracking changes in sea ice, vegetation, and glacier dynamics.

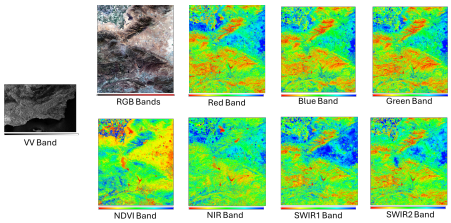

(a) Multispectral RGB composite and analysis of sea ice and vegetation in the Arctic region (September 2024). Various bands are used for assessing vegetation health, sea ice extent, and surface features.

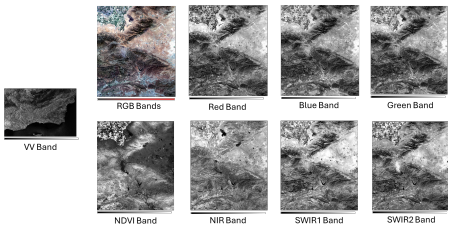

(b) SAR VV polarization image of the Arctic region (September 2024). Dark areas indicate smoother ice surfaces, while brighter regions reveal rough glacial terrain and permafrost.

Fig. 2.5 Combined analysis of the Arctic region using SAR and multispectral data from September 2024. The RGB composite reveals sea ice extent and vegetation changes, while SAR data highlights surface roughness, glacier dynamics, and permafrost characteristics.

Figure 2.5 illustrates how SAR and multispectral data are used to monitor sea ice extent, vegetation changes, and glacier dynamics in the Arctic, providing valuable information for understanding the impacts of climate change.

2.5 Conclusion

This chapter highlighted the value of EO data, enhanced by spatial, spectral, temporal, and radiometric resolutions for improved data quality. Combining SAR and multispectral data enables effective monitoring in challenging conditions [37].

AI techniques like Compressive Sensing (CS), ML, and DL are essential for managing large datasets and addressing noise.

Case studies on volcanic activity and Danube Delta monitoring show EO's practical benefits, highlighting the need for high-resolution data in climate, disaster, and resource management [39, 25].

Future EO progress will depend on AI frameworks to fully harness growing data volumes [13].

Chapter 3

Processing Chain of Earth Observation

3.1 Importance and Overview of Data Processing in RS

The Earth observation processing chain converts raw data into actionable insights, encompassing calibration, core analysis, and finalization, with SNAP software as a key tool.

3.1.1 Data Calibration and Preprocessing

Calibration and preprocessing ensure accuracy, correcting distortions in raw data. SNAP enhances data reliability through precise calibration, critical for applications like vegetation monitoring [19].

3.1.2 Core Analysis

Core analysis extracts information using SNAP tools. Feature extraction and classification techniques, such as NDVI and SVM, aid in analyzing land cover and vegetation [33].

3.1.3 Finalization

Finalization includes validating results, integrating data, and generating outputs like NDVI maps for decision-making [5].

3.2 Overview of SNAP

SNAP, developed by ESA, processes data from sources like Sentinel and Landsat missions, offering tools for data manipulation and advanced analysis [28].

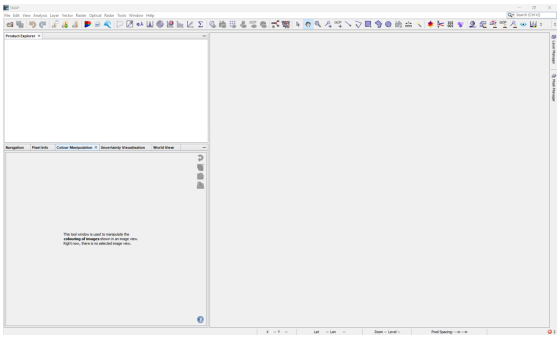

Fig. 3.1 The SNAP interface environment showing tools for data manipulation, color manipulation, and advanced remote sensing processing.

3.2.1 Supported Missions and Multi-Mission Capability

SNAP's multi-mission capability allows processing data from multiple sensors, like radar from Sentinel-1 and optical from Sentinel-2, facilitating multi-sensor research in climate and environmental studies [28].

3.2.2 Co-Registration of Sentinel-1 and Sentinel-2 Data Using SNAP

Co-registration aligns Sentinel-1 and Sentinel-2 imagery for change detection, data fusion, and time-series analysis.

Sentinel-1 GRD Processing Workflow in SNAP

The Sentinel-1 GRD workflow includes steps like applying an orbit file to correct satellite trajectory, improving geometric accuracy for analysis.

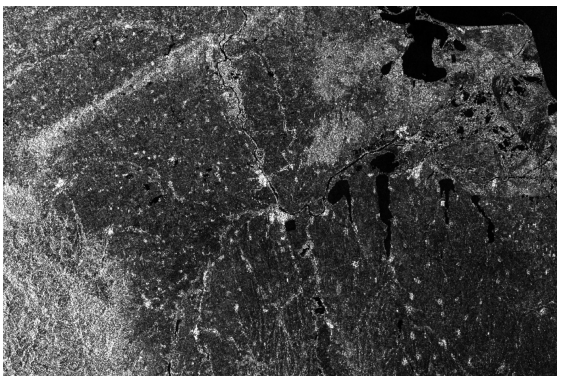

Fig. 3.2 Application of the orbit file in SNAP to improve geometric accuracy of Sentinel-1 GRD data.

3.2.3 Thermal Noise Removal

Thermal noise, which degrades data quality, is removed to ensure the backscatter signal accurately represents surface properties.

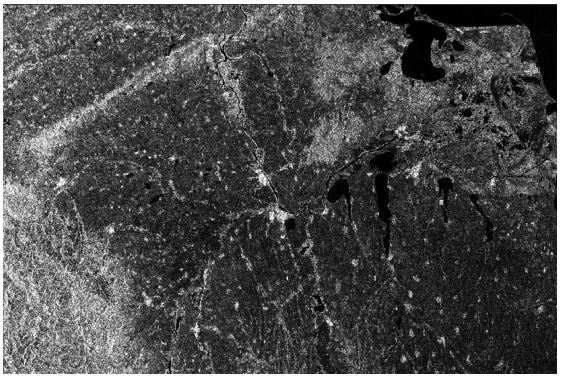

Fig. 3.3 Thermal noise removal applied to Sentinel-1 data using SNAP.

3.2.4 Border Noise Removal

Border noise is removed to clean up SAR images and improve usability.

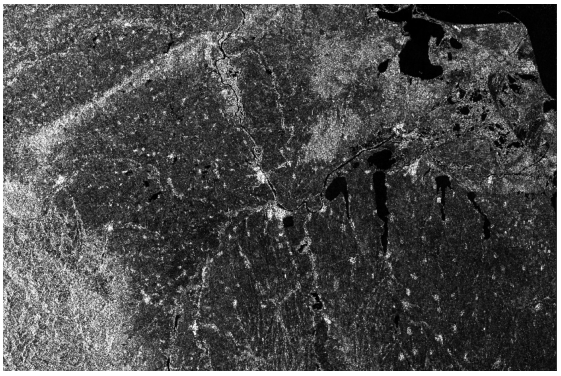

Fig. 3.4 Removing border noise from Sentinel-1 GRD data using SNAP.

3.2.5 Radiometric Calibration

Radiometric calibration converts digital numbers into backscatter coefficients (σ^0), ensuring data is quantitatively comparable.

3.2.6 Terrain Correction

Terrain correction uses a DEM to adjust pixel coordinates, ensuring features in SAR images are correctly mapped to their geographic positions.

3.2.7 Convert Bands to dB

Converting SAR data from linear scale to decibels (dB) simplifies interpretation and comparison across datasets.

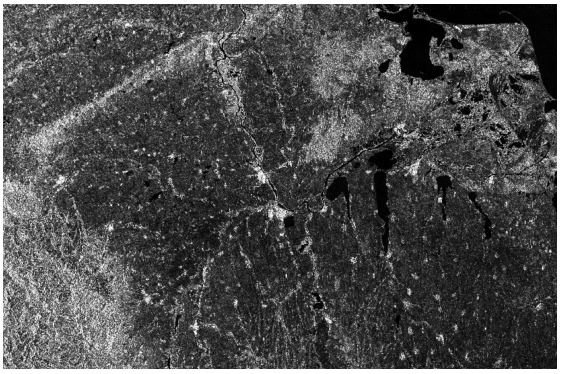

Fig. 3.5 Radiometric calibration applied to Sentinel-1 data, converting pixel values into backscatter coefficients (σ^0).

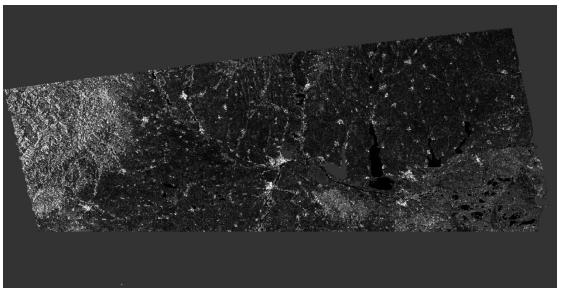

Fig. 3.6 Terrain correction in SNAP uses a DEM to adjust for topographic distortions in Sentinel-1 SAR data.

3.2.8 Subset

The subset function reduces data volume and processing time by focusing on the area of interest.

Sentinel-2 Preprocessing Workflow in SNAP

Sentinel-2 preprocessing includes similar steps, such as subsetting and collocation, to prepare data for analysis.

3.2.9 Subset

Subsetting Sentinel-2 data reduces dataset size by focusing on the area of interest.

3.2.10 Collocation

Collocation aligns Sentinel-1 SAR data and Sentinel-2 optical imagery for joint analysis.

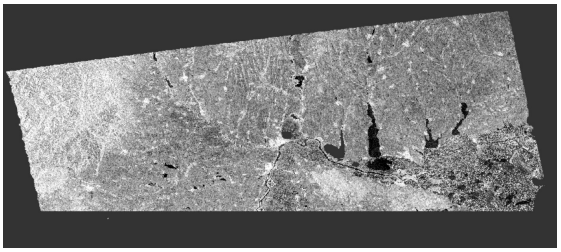

Fig. 3.7 Conversion of backscatter values from linear to decibel (dB) scale in SNAP.

Fig. 3.8 Subsetting Sentinel-1 GRD data in SNAP.

3.3 Introduction to CS

Compressed Sensing (CS) efficiently acquires and reconstructs signals by leveraging sparsity, reducing data volume while maintaining crucial information, making it suitable for handling large datasets from SAR and hyperspectral sensors [11].

3.3.1 Origins and Development

CS was developed in the early 2000s by Candès, Romberg, Tao, and Donoho, showing that sparse signals could be reconstructed with fewer samples [8, 14].

3.3.2 Core Concepts and Mathematical Foundation

CS relies on sparsity and incoherence. The measurement vector y is represented as $y = \Phi x$, where x is the sparse signal, and Φ is the sensing matrix. The reconstruction problem is solved using optimization techniques, such as Basis Pursuit [9, 14].

3.4 Overview of AI Techniques

AI techniques, particularly ML and DL, have transformed RS by simplifying complex workflows, enhancing efficiency, and extracting deeper insights from satellite data. These capabilities are crucial for real-time applications like disaster management and land-use classification [5].

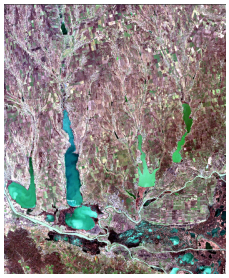

Fig. 3.9 Subsetting Sentinel-2 data in SNAP.

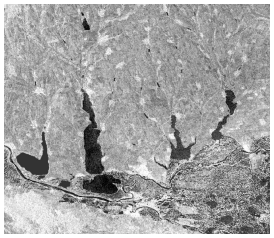

(a) Sentinel-1 VV band data.

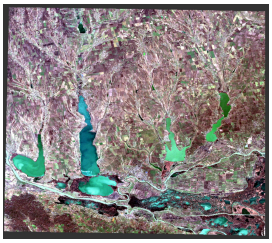

(b) Sentinel-2 RGB data.

Fig. 3.10 Collocated Sentinel-1 VV band and Sentinel-2 RGB images for multi-sensor analysis.

3.4.1 ML in RS

ML automates data analysis, with supervised learning (e.g., SVM, Random Forests) for tasks like land cover classification, and unsupervised learning (e.g., K-means, PCA) for image segmentation and anomaly detection [23, 2].

3.4.2 DL in RS

DL models, such as CNNs, are widely used for tasks like land cover classification and object detection in satellite images [21, 41].

3.5 Thesis Approach

This thesis aims to improve EO data processing accuracy and efficiency using CS, ML, and DL. Applied to tasks in the Danube Delta, including land cover analysis, temporal changes, and ship detection, these techniques address challenging RS environments.

In land cover analysis, CS reduces data volume, while ML and DL enable automated feature extraction. Temporal changes are tracked through co-registered Sentinel-1 and Sentinel-2 data with AI techniques like clustering and SVM. SAR ship detection employs DL models like YOLO for high accuracy, with CS minimizing redundancy.

This integration offers scalable, accurate solutions for EO, supporting real-time processing and decision-making.

Chapter 4

Summarized Chapter 4: Analyzing Temporal Changes in the Danube Delta

4.1 Abstract

Classifying remote sensing (RS) imagery in dynamic areas like the Danube Delta is challenging due to rapid landscape changes [18]. This study utilizes co-registered synthetic aperture radar (SAR) and multispectral (MS) data, applying machine learning (ML) techniques—t-SNE, K-means clustering [20], and SVM classification [27]. Results show that the SAR VV band provides detailed training data [34], while MS's infrared band aids in reference extraction [29]. An SVM model enhanced by t-SNE achieved 91.60% accuracy, supporting effective monitoring of the Danube Delta's dynamic environment [26].

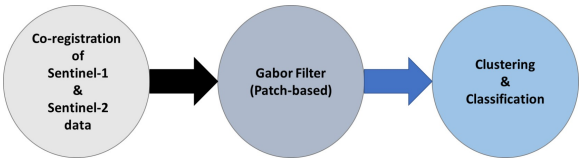

Fig. 4.1 The block diagram of the project is categorized into three main sections, including co-registration of SAR and MS data; applying the Gabor filter on extracted patches; and clustering and classification techniques, respectively.

4.2 Introduction

Remote sensing (RS) image classification is crucial for environmental monitoring, especially in dynamic areas like the Danube Delta, which faces threats of biodiversity loss [18]. Combining synthetic aperture radar (SAR) and multispectral (MS) imagery with co-registration provides a comprehensive view of environmental changes [34, 26].

Fig. 4.2 The study's ROI is situated within the Danube Delta, at the border between southeastern Romania and southern Ukraine.

This study employs machine learning (ML) techniques—Gabor filters for feature extraction [22], K-means for unsupervised classification [20], and SVM for supervised classification [27]—to monitor temporal changes in the Delta, facilitating efficient tracking of its ecological patterns.

4.3 Methodology

Co-registered SAR and MS data from the Copernicus Open Access Hub, spanning ten months, were used to capture seasonal and long-term changes. Preprocessing in SNAP included orbit correction, noise removal, calibration, and terrain correction. Gabor filters were applied for feature extraction, enhancing texture representation.

K-means clustering and t-SNE grouped features into three categories: water bodies, land, and vegetation. t-SNE reduced high-dimensional data for visualization, while SVM performed supervised classification to distinguish between the classes.

4.3.1 Patch Extraction and Gabor Feature Representation

Gabor filters were applied to segmented patches, producing a 48-dimensional feature vector for classification through various orientations and scales.

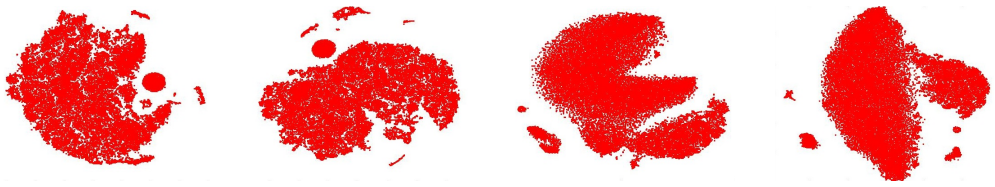

(a) t-SNE on RGB (b) t-SNE on Infrared (c) t-SNE on VV (d) t-SNE on VH

Fig. 4.3 Results from applying t-SNE on feature vectors for four different bands: RGB, Infrared, VV, and VH, respectively. The SAR VV band performed the best, showing clear separation into three classes.

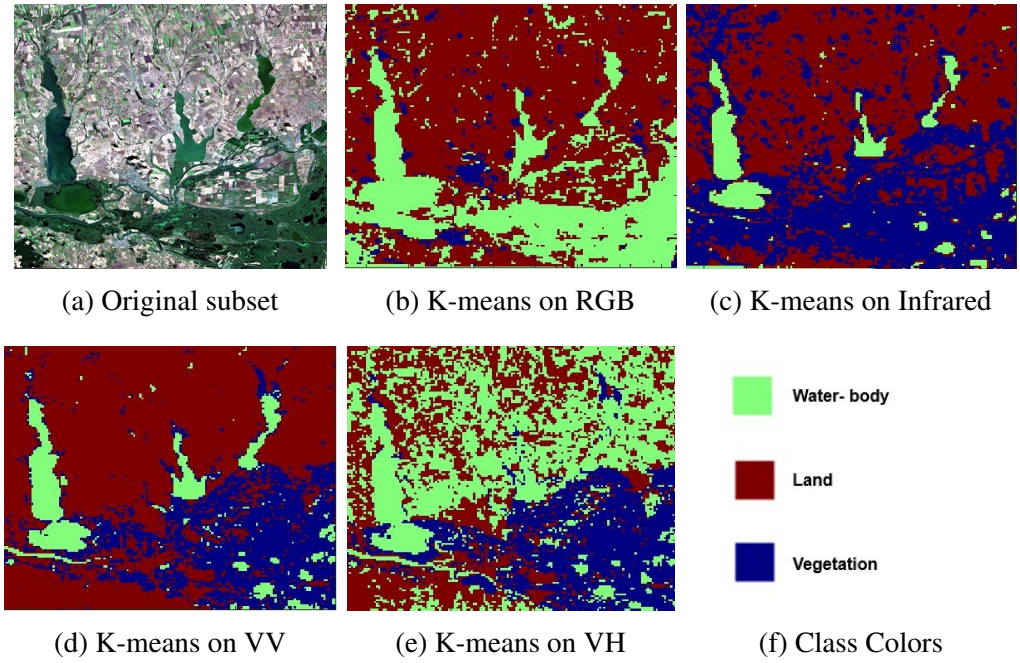

(a) Original subset (b) K-means on RGB (c) K-means on Infrared

(d) K-means on VV (e) K-means on VH (f) Class Colors

Fig. 4.4 The original subset (a) and clustering results on four different bands—RGB, Infrared, VV, and VH—after applying K-means for three classes: water-body, land, and vegetation. The MS Infrared and SAR VV bands provided the best clustering results.

4.3.2 Clustering by K-means

Figure 4.3 shows t-SNE visualization of feature vectors from SAR and MS bands, with SAR VV best categorizing three classes. Figure 4.4 illustrates K-means clustering, effectively distinguishing water, land, and vegetation.

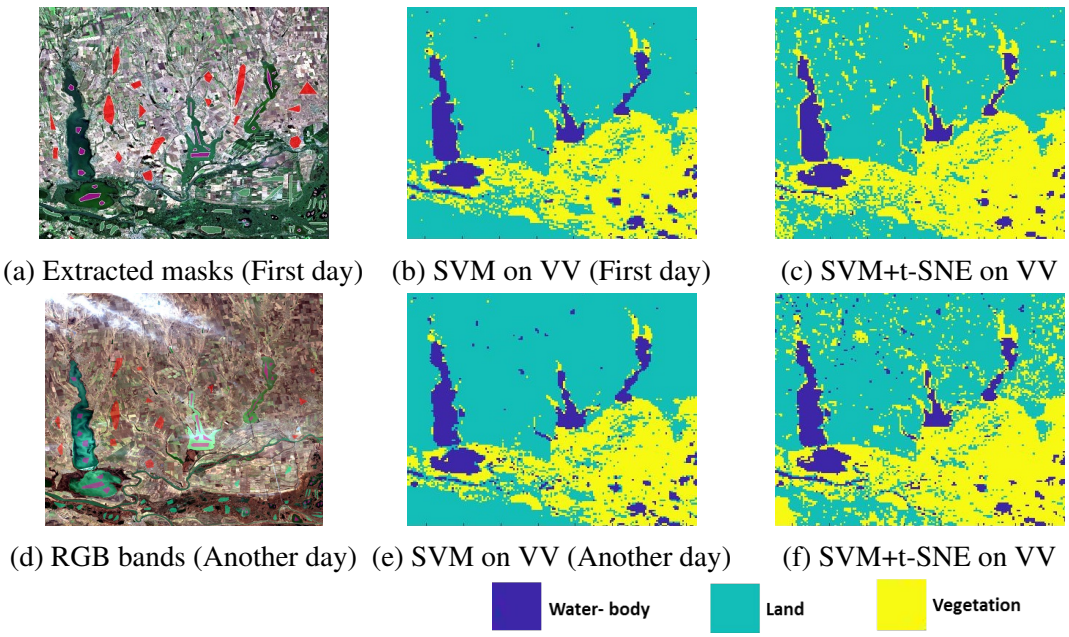

(a) Extracted masks (First day) (b) SVM on VV (First day) (c) SVM+t-SNE on VV

(d) RGB bands (Another day) (e) SVM on VV (Another day) (f) SVM+t-SNE on VV

Fig. 4.5 SVM classification on the SAR VV band, comparing results on two different dates. SVM+t-SNE demonstrates enhanced classification accuracy.

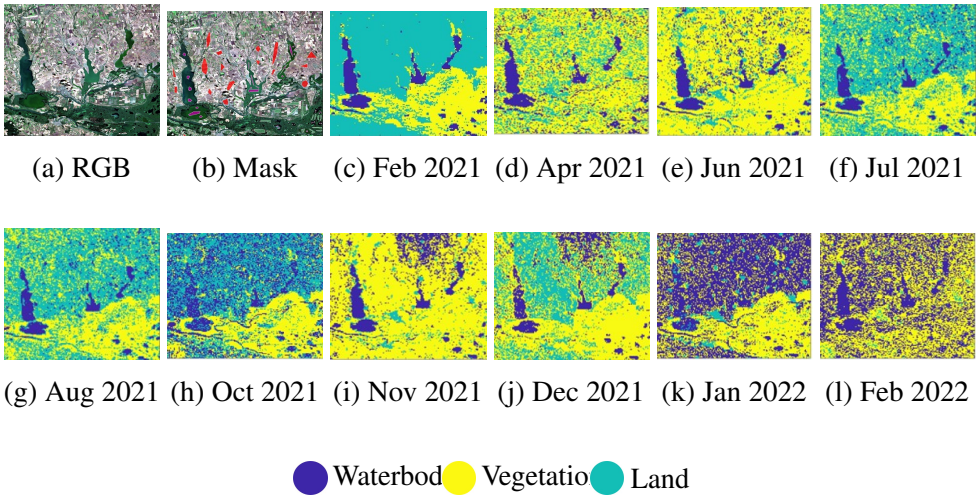

Fig. 4.6 A collection of RGB images, masks, and feature maps over various months from February 2021 to February 2022.

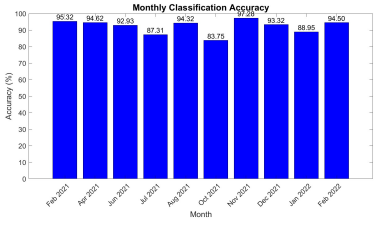

Fig. 4.7 Classification Accuracy

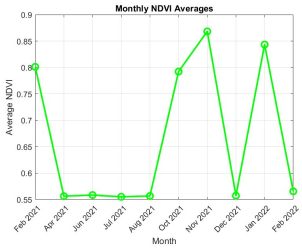

Fig. 4.8 NDVI Averages

Fig. 4.9 Side-by-side comparison of Classification Accuracy and NDVI Averages

4.3.3 Supervised Classification by SVM

SVM classified SAR VV band features. Figure 4.5 shows improved accuracy when t-SNE was used before training.

4.4 Results on Time Series Data

SVM classified land, vegetation, and water bodies consistently over ten dates. Figure 4.6 shows land cover distribution across time.

4.5 Conclusion

Combining SAR and MS data with ML models supports accurate monitoring in the Danube Delta. t-SNE integration with SVM improves classification accuracy. Future work will extend to more classes and deep learning methods.

Chapter 5

Goal-Oriented Semantic Modules for SAR Ship Detection

Abstract

This chapter introduces a novel methodology for SAR ship detection, combining Convolutional Neural Networks (CNNs) [21, 41] and Vision Transformers (ViTs) [15] with a gating mechanism. Initially validated on the MNIST dataset [12] and then on SAR ship detection data (PSeg-SSDD) [42], the methodology shows robustness and versatility. A modified YOLOv5s model [38] provides a balanced trade-off between accuracy and computational efficiency, demonstrating its practical application in maritime surveillance.

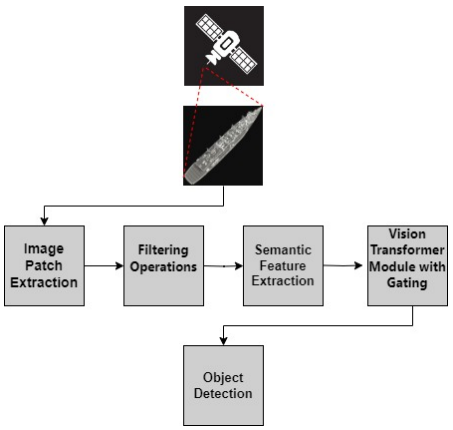

Fig. 5.1 Schematic Representation of the Proposed Methodology

5.1 Introduction

Synthetic Aperture Radar (SAR) technology revolutionizes maritime surveillance by enabling ship detection under all weather conditions, day or night [41]. Unlike optical sensors, SAR relies on microwave signals, allowing detection through clouds and darkness [34]. This capability supports maritime traffic management, border protection, and environmental conservation. Despite its advantages, SAR-based ship detection encounters challenges due to noise and complex environments [10]. Figure 5.1 illustrates the proposed methodology, showcasing the integration of Convolutional Neural Networks (CNNs) [21] and Vision Transformers (ViT) [15] for ship detection tasks, enhancing feature perception through a gating mechanism.

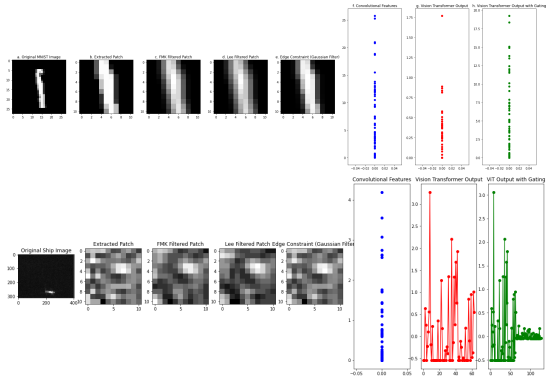

Fig. 5.2 Feature extraction and fusion process on images from the MNIST dataset and SAR ship detection data, demonstrating adaptability of CNN and ViT models across domains.

5.2 Methodology

The approach integrates CNNs and ViTs, combined with a gating mechanism, and optimized within the YOLOv5s framework. Figure 5.2 illustrates the feature extraction process on the MNIST and SAR datasets, highlighting each transformation step, from patch extraction to ViT output with gating, which adapts the model for varied maritime conditions.

5.2.1 Data Preprocessing

The PSeg-SSDD dataset was processed to enhance image quality. This involved noise reduction using FMK and Lee filters, edge enhancement, and normalization to optimize SAR data for DL models. The dataset was divided into training, validation, and testing, ensuring comprehensive evaluation.

5.2.2 YOLOv5s Model Structure

YOLOv5s is structured with three main components: Backbone, Neck, and Head, each optimized for efficient object detection. The modified model integrates EfficientConvModule and SE blocks, as shown in Figure 6.2, to improve detection accuracy and efficiency.

5.3 Experimental Results

The approach was validated on MNIST and SAR ship detection datasets, achieving a mean Average Precision (mAP) of 96% at an IoU threshold of 0.5 on SAR data. Figure 6.3 shows performance across various evaluation metrics, with consistent high precision and recall.

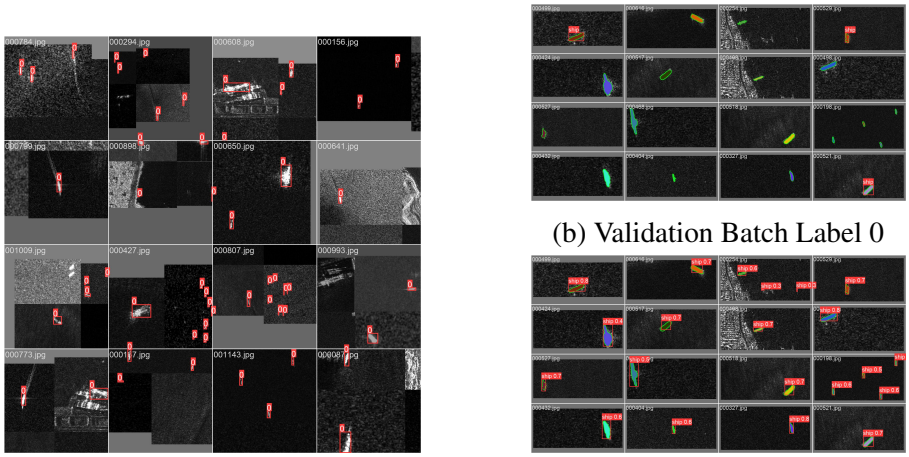

(a) Train Batch 0

(b) Validation Batch Label 0

(c) Validation Batch Prediction 0

Fig. 5.3 Training and validation stages for SAR ship detection using YOLOv5s on PSeg-SSDD dataset.

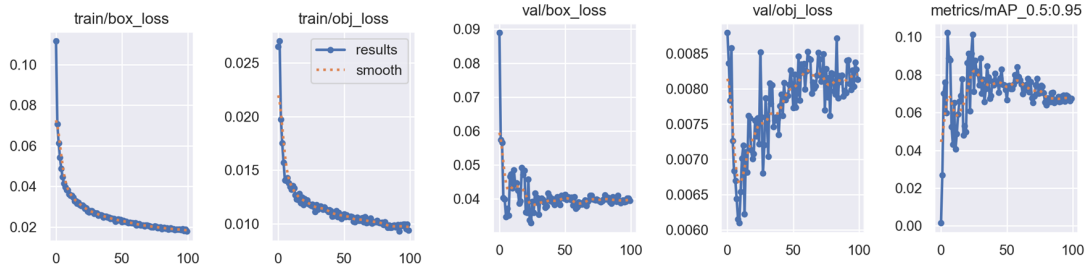

Fig. 5.4 Results via different parameters and metrics.

5.4 Conclusion

This chapter presents an effective SAR ship detection methodology integrating CNNs, ViTs, and enhancements in the YOLOv5s architecture. Future research will expand its applications to environmental monitoring and other remote sensing tasks.

Chapter 6

Compressive SAR Learning

Abstract

Compressive Learning (CL) for SAR reduces data requirements, enhancing efficiency and lowering computational demands. The first method combines signal processing with Compressive Sensing (CS) to achieve 80% accuracy with minimal measurements [1], while the second uses joint end-to-end training for improved accuracy on reduced datasets [24].

ompressive Learning (CL), Synthetic Aperture Radar (SAR), Data Reduction, Joint Signal Processing, CS Framework, SVM Classifier, Binary Sensing Matrix.

6.1 Introduction

CL leverages signal sparsity to reconstruct data from fewer measurements [6]. In SAR imaging, combining sparse imaging with ML enables tasks like recognition and classification [41]. Previous studies have used CS algorithms like MRKCS and ITR to improve SAR data compression [4]. SAR sensors, using microwave signals, are critical in remote sensing (RS) for continuous imaging [30]. CS methods reduce data requirements, lowering RS storage and transmission needs [9]. Integrating CL with SAR enhances tasks like classification, advancing sparse representation research [11].

CL's effectiveness in SAR is demonstrated through joint training of sensing matrices and classifiers, which boosts classification accuracy [24]. Experiments with fixed and trainable matrices confirm CL's potential to optimize SAR data processing [14].

6.2 Methodology

This study proposes compressing SAR data via linear transformations and classifying it without reconstruction. Figure 6.1 illustrates the framework with three scenarios: (I) fixed sensing matrix with classifier, (II) fixed sensing matrix with decoder, and (III) trainable sensing matrix with joint classifier and decoder training.

6.2.1 Compression and Sensing Matrix Construction

Compression was achieved by reducing measurements using a random matrix, denoted by A, chosen from Binary, Gaussian, or Uniform distributions.

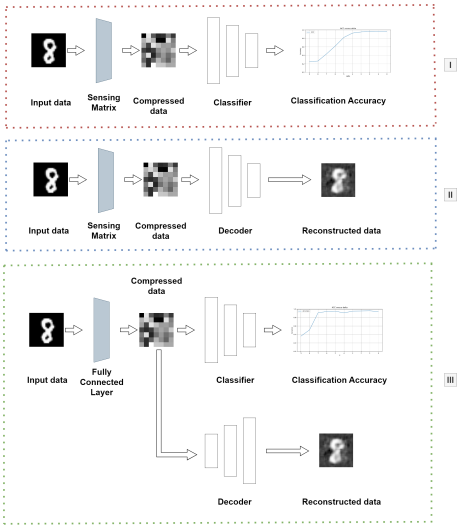

Fig. 6.1 The block diagram of the proposed method.

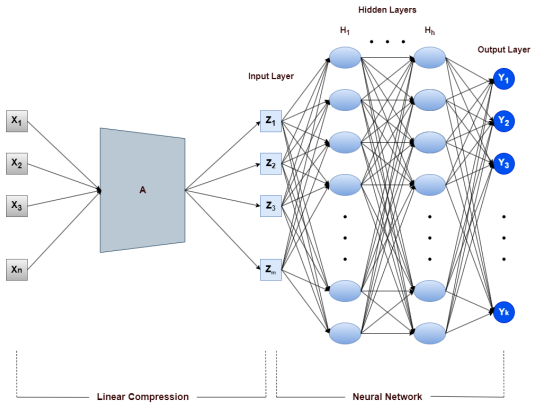

Fig. 6.2 The block diagram of the proposed method includes three different scenarios: (I) fixed sensing matrix plus classifier, (II) fixed sensing matrix plus decoder, and (III) trainable sensing matrix with joint training of both classifier and decoder.

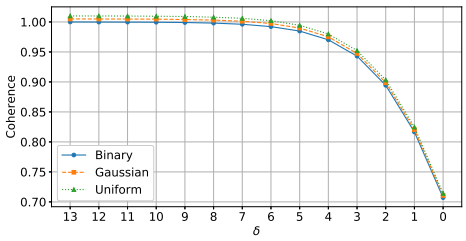

Fig. 6.3 Comparison of coherence for three distinct distributions: Uniform, Gaussian, and Binary, across varying values of δ.

6.2.2 Classification and Trainable Matrix

Classifiers used include MLP, RF, and SVM, selected based on dataset characteristics. Additionally, a trainable sensing matrix was integrated, allowing for optimization through joint training. This method retained more crucial data in compressed measurements, enhancing classification accuracy.

6.3 Experiments

6.3.1 Datasets and Training

Experiments used MNIST and MSTAR datasets, employing an MLP model trained in Pytorch.

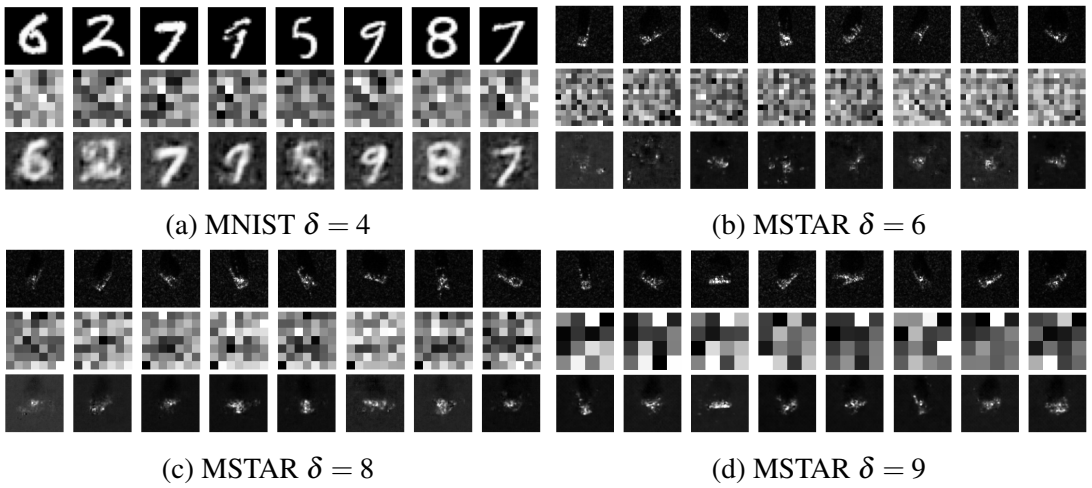

(a) MNIST $\delta = 4$ (b) MSTAR $\delta = 6$

(c) MSTAR $\delta = 8$ (d) MSTAR $\delta = 9$

Fig. 6.4 Original data, compressed data, and reconstructed data

6.4 Results

6.4.1 Classification and Reconstruction Performance

Higher compression levels reduced classification accuracy, as shown in Figure 6.6. Reconstruction results in Figure 6.4 confirm that compressed data retains essential information even at high compression, suitable for applications with limited storage.

6.4.2 Joint Training

Joint training outperformed fixed matrix setups, especially in the MNIST and MSTAR datasets, as shown in Figure 6.7. This approach allows the sensing matrix to adapt, optimizing classification and reconstruction together.

6.5 Conclusion

CL enhances SAR data efficiency, significantly reducing data requirements while maintaining classification performance. The study demonstrated joint training's impact on accuracy, promoting CL as a viable solution for RS and SAR applications with data constraints. Future research should further optimize CL for broader SAR datasets.

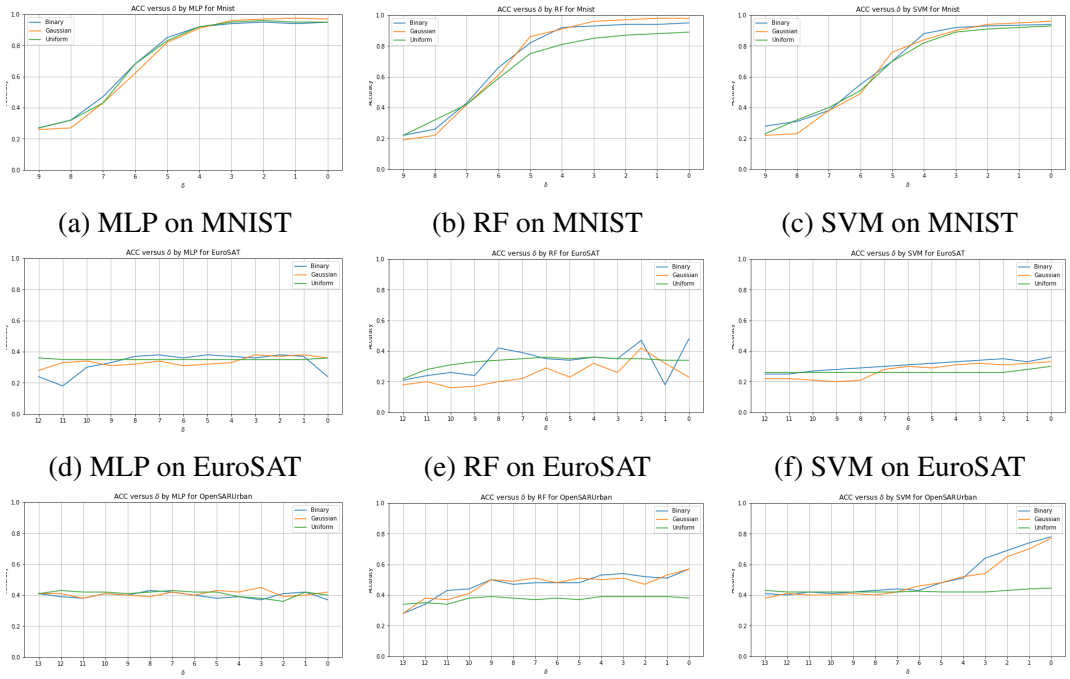

(a) MLP on MNIST (b) RF on MNIST (c) SVM on MNIST

(d) MLP on EuroSAT (e) RF on EuroSAT (f) SVM on EuroSAT

(g) MLP on OpenSARUrban (h) RF on OpenSARUrban (i) SVM on OpenSARUrban

Fig. 6.5 Accuracy versus δ plots for different classifiers and sensing matrix types on the three different datasets including MNIST, EuroSAT, and OpenSARUrban.

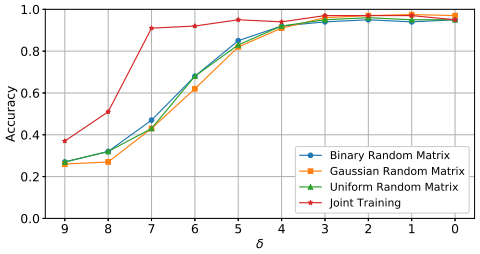

Fig. 6.6 The classification accuracy curve versus different δ for the MNIST dataset.

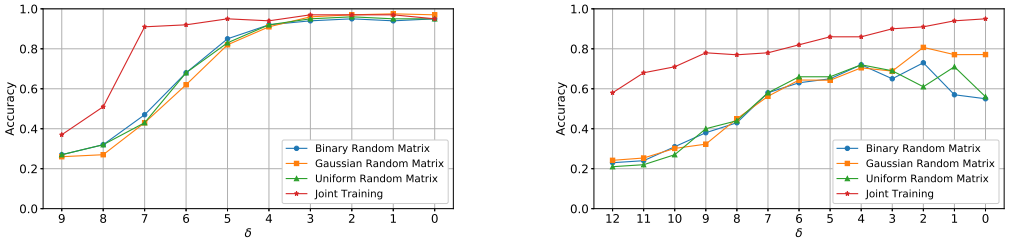

(a) MNIST (b) MSTAR

Fig. 6.7 The classification accuracy curves versus different δ for joint training and a fixed sensing matrix with different distributions.

Chapter 7

Conclusions

This thesis enhances SAR data processing and multispectral fusion for EO applications using compressive sensing (CS) and AI/ML. Key contributions include:

- A CS framework reducing data acquisition for real-time SAR monitoring.
- AI/ML techniques (CNNs, SVM, t-SNE) for feature extraction and classification.
- SAR-MS co-registration validated in the Danube Delta.
- Time-series analysis for monitoring vegetation and land use.

7.1 Main Contributions

This work improves EO data processing by:

- Developing an efficient CS framework for SAR.
- Advancing SAR-MS analysis with AI/ML for classification.
- Proposing a validated SAR-MS co-registration method.
- Expanding into time-series analysis for long-term monitoring.

7.2 Publications

7.2.1 Journal Articles

- Keymasi, M., et al., **"Compressive SAR Learning,"** *Sensors*, Special Issue on "Innovations in Photogrammetry and Remote Sensing," 2024.

7.2.2 Conference Proceedings

- Keymasi, M., et al., **"Classification of Danube Delta Boundaries by Using Machine Learning Algorithms on Co-registered Sentinel-1 and Sentinel-2 Data,"** *Advanced Topics in Optoelectronics, Microelectronics, and Nanotechnologies XI*, 2023.
- Keymasi, M., et al., **"An Efficient Compressive Learning Method on Earth Observation Data,"** *IGARSS 2023*, IEEE, 2023.
- Keymasi, M., and Datcu, M., **"Analyzing Temporal Changes in the Danube Delta: A Time Series Study with Co-registered Sentinel-1 and Sentinel-2 Data,"** *ATOMS 2024 Conference*.
- Keymasi, M., et al., **"Goal-Oriented Semantic Modules for SAR Ship Detection,"** *CoSeRa 2024 Conference*.
- Keymasi, M., et al., **"Hybrid GAN and Fourier Transformation for SAR Ocean Pattern Image Augmentation,"** *IEEE MetroSea 2024*.

7.3 Future Work

Future directions include:

- **Noise Resistance**: Develop robust CS algorithms.
- **Real-Time Processing**: Leverage cloud/edge computing.
- **Quantum and AI**: Use quantum computing for faster SAR analysis.
- **Extended Time-Series Applications**: Apply to urban and climate studies.
- **Enhanced Data Fusion**: Integrate data from sensors like LiDAR.

These directions aim to advance SAR processing and EO applications.

References

[1] Baraniuk, R. G. (2007). Compressive sensing [lecture notes]. *IEEE Signal Processing Magazine*, 24(4):118–121.

[2] Belgiu, M. and Drăguţ, L. (2016). Random forest in remote sensing: A review of applications and future directions. *ISPRS Journal of Photogrammetry and Remote Sensing*, 114:24–31.

[3] Blaschke, T. (2010). Object based image analysis for remote sensing. *ISPRS Journal of Photogrammetry and Remote Sensing*, 65(1):2–16.

[4] Calderbank, R., Jafarpour, S., and Schapire, R. (2009). Compressed learning: Universal sparse dimensionality reduction and learning in the measurement domain. *Preprint*.

[5] Campbell, J. B. and Wynne, R. H. (2011). *Introduction to Remote Sensing*. Guilford Press, New York, 5th edition.

[6] Candes, E. (2006). Compressive sampling. 3:1433–1452.

[7] Candes, E. and Tao, T. (2005). Decoding by linear programming. *IEEE Transactions on Information Theory*, 51(12):4203–4215.

[8] Candès, E. J., Romberg, J. K., and Tao, T. (2006). Stable signal recovery from incomplete and inaccurate measurements. *Communications on Pure and Applied Mathematics*, 59(8):1207–1223.

[9] Candès, E. J. and Tao, T. (2006). Near-optimal signal recovery from random projections: Universal encoding strategies? *IEEE Transactions on Information Theory*, 52(12):5406–5425.

[10] Cetin, M. and Karl, W. C. (2014). Sparsity-driven synthetic aperture radar imaging: Reconstruction, robustness, and model uncertainty. *IEEE Signal Processing Magazine*, 31(4):27–40.

[11] Davenport, M. A., Wakin, M. B., Duarte, M. F., and Baraniuk, R. G. (2010). Introduction to compressive sensing. *IEEE Signal Processing Magazine*, 25(2):21–30.

[12] Deng, L. (2012). The mnist database of handwritten digit images for machine learning research [best of the web]. *IEEE Signal Processing Magazine*, 29(6):141–142.

[13] Doe, J. and Smith, J. (2021). Future directions in earth observation technology. *International Journal of Remote Sensing*.

[14] Donoho, D. L. (2006). Compressed sensing. *IEEE Transactions on Information Theory*, 52(4):1289–1306.

[15] Dosovitskiy, A., Beyer, L., Kolesnikov, A., et al. (2021). An image is worth 16x16 words: Transformers for image recognition at scale. In *International Conference on Learning Representations*.

[16] Drusch, M., Del Bello, U., Carlier, S., et al. (2012). Sentinel-2: Esa's optical high-resolution mission for gmes operational services. *Remote Sensing of Environment*, 120:25–36.

[17] (ESA), E. S. A. (2020). Synthetic aperture radar: Remote sensing applications. *ESA Publications*. Accessed on 2023-10-15.

[18] Finkl, C. and Makowski, C. (2022). Identification of domain complexes in the danube delta coastal belt using the biophysical cross-shore classification system (bccs), based on interpretation of satellite imagery. *Journal of Coastal Research*, 38(1):1–18.

[19] Jensen, J. R. (2007). *Remote Sensing of the Environment: An Earth Resource Perspective*. Pearson, Upper Saddle River, NJ, 2nd edition.

[20] Lloyd, S. (1982). Least squares quantization in pcm. *IEEE Transactions on Information Theory*, 28(2):129–137.

[21] Maggiori, E. et al. (2017). Convolutional neural networks for large-scale remote-sensing image classification. *IEEE Transactions on Geoscience and Remote Sensing*, 55(2):645–657.

[22] Manjunath, B. and Ma, W. (1996). Texture features for browsing and retrieval of image data. *IEEE Transactions on Pattern Analysis and Machine Intelligence*, 18(8):837–842.

[23] Melgani, F. and Bruzzone, L. (2004). Classification of hyperspectral remote sensing images with support vector machines. *IEEE Transactions on Geoscience and Remote Sensing*, 42(8):1778–1790.

[24] Mousavi, A., Patel, V. M., and Baraniuk, R. G. (2015). Deep learning for compressive sensing. *IEEE Transactions on Signal Processing*, 63(22):6001–6014.

[25] Niculescu, S., B. J. and Lardeux, C. (2020). Synergy of high-resolution radar and optical images for mapping wetland macrophytes on the danube delta. In *Remote Sensing Symposium*, volume 12, page 2188.

[26] Niculescu, S., Boissonnat, J., Lardeux, C., Roberts, D., Hanganu, J., et al. (2020). Synergy of high-resolution radar and optical images satellite for identification and mapping of wetland macrophytes on the danube delta. *Remote Sensing*, 12(14):2188.

[27] Pal, M. and Mather, P. (2005). Support vector machines for classification in remote sensing. *International Journal of Remote Sensing*, 26(5):1007–1011.

[28] Patrick Helber, Benjamin Bischke, A. D. and Borth, D. (2019). *EuroSAT: A novel dataset and deep learning benchmark for land use and land cover classification*, volume 12. IEEE.

[29] Richards, J. A. (2013). Remote sensing digital image analysis.

[30] Schmitt, M. et al. (2016). Data fusion and integration for multitemporal and multimodal remote sensing: A review of concepts and methods. *Proceedings of the IEEE*, 104(9):1615–1627.

[31] Schmitt, M. and Zhu, X. (2016). Data fusion and remote sensing: An ever-growing relationship. *IEEE Geoscience and Remote Sensing Magazine*, 4(4):6–23.

[32] Singh, A. (1989). Digital change detection techniques using remotely sensed data. *International Journal of Remote Sensing*, 10(6):989–1003.

[33] Thomas Lillesand, R. W. K. and Chipman, J. (2015). Remote sensing and image interpretation.

[34] Torres, R., Snoeij, P., Geudtner, D., et al. (2012). Gmes sentinel-1 mission. *Remote Sensing of Environment*, 120:9–24.

[35] Tucker, C. J. (1986). Satellite remote sensing of vegetation. In *Annual Review of Ecology and Systematics*, pages 379–393.

[36] Veci, L. (2016). Sentinel-1 toolbox sar processing algorithms. Technical report.

[37] Wang, L. and Yao, M. (2022). Sar and multispectral data integration. *Journal of Applied Remote Sensing*.

[38] Wang, S., Gao, S., Zhou, L., Liu, R., Zhang, H., Liu, J., Jia, Y., and Qian, J. (2022). Yolo-sd: Small ship detection in sar images by multi-scale convolution and feature transformer module. *Remote Sensing*, 14(20):5268.

[39] Xie, F., L. B. and Liu, Y. (2022). Research on the coordinate attention mechanism fuse in a yolov5 deep learning detector for the sar ship detection task. *Sensors*, 22(3370):1–15.

[40] Ye, Y., Yang, C., Zhu, B., Zhou, L., He, Y., and Jia, H. (2021). Improving co-registration for sentinel-1 sar and sentinel-2 optical images. *Remote Sensing*, 13(5):928.

[41] Zhang, J., Shi, G., Liu, B., Yang, Y., and Xing, X. (2019). Sar ship detection using deep learning: A review. *IEEE Geoscience and Remote Sensing Letters*, 16(8):1200–1204.

[42] Zhang, T., Zhang, X., Li, J., Xu, X., Wang, B., Zhan, X., Xu, Y., Ke, X., Zeng, T., Su, H., et al. (2021). Sar ship detection dataset (ssdd): Official release and comprehensive data analysis. *Remote Sensing*, 13(18):3690.

[43] Zhu, X. X. et al. (2017). Deep learning in remote sensing: A comprehensive review and list of resources. *IEEE Geoscience and Remote Sensing Magazine*, 5(4):8–36.